Supporting Information: Elementary Decomposition Mechanisms of Lithium Hexafluorophosphate in Battery Electrolytes and Interphases

Evan Walter Clark Spotte-Smith,[†,‡,⊥] Thea Bee Petrocelli,[†,‡,¶,⊥] Hetal D. Patel,[†,‡] Samuel M. Blau,[§] and Kristin A. Persson[*,‡,‖]

†*Materials Science Division, Lawrence Berkeley National Laboratory, 1 Cyclotron Road, Berkeley, CA, 94720 USA*

‡*Department of Materials Science and Engineering, University of California, Berkeley, 210 Hearst Memorial Mining Building, Berkeley, CA, 94720 USA*

¶*Cabrillo College, 6500 Soquel Drive, Aptos, CA, 95003 USA*

§*Energy Storage and Distributed Resources, Lawrence Berkeley National Laboratory, 1 Cyclotron Road, Berkeley, CA, 94720 USA*

‖*Molecular Foundry, Lawrence Berkeley National Laboratory, 1 Cyclotron Road, Berkeley, CA, 94720 USA*

⊥*These authors contributed equally to this work*

E-mail: kapersson@lbl.gov

Data availability

We have distributed data for this work as a JavaScript Object Notation (JSON)-formatted file `pfx_named_data.json` on Figshare (DOI:10.6084/m9.figshare.21583581.v1).[1]

`pfx_named_data.json` contains the structures (as serialized Pymatgen[2] `Molecule` objects) and thermochemical properties of the reaction endpoints and TS reported in this work. The key for each key-value pair in `pfx_named_data.json` is the name of the species as reported in the main text or this Supporting Information. For instance, the data for TS_{11} would be found under the key "TS11". For reactions where species, namely LiF, HF, and CO_2, are removed (see details below), two entries for the relevant endpoint are provided. The species with LiF, HF, and/or CO_2 present are named "Mn", where n is the appropriate index; the species with the species removed are named "Mn-x", where x is the species that is removed. Where multiple species are removed, the name takes the form "Mn-x-y", where x and y are the species removed.

To load this data in Python, use monty (https://github.com/materialsvirtuallab/monty):

```
from monty.serialization import loadfn
data = loadfn("pfx_named_data.json")
```

Computational methods

Transition-states (TS) were identified using the AutoTS algorithm[3] which relies on the Jaguar electronic structure code.[4] In cases where AutoTS could not identify a TS, the single-ended growing string method (SE-GSM)[5] was used. Specifically, the pyGSM implementation of SE-GSM[6] was used with the Q-Chem electronic structure code version 5.4.2 as the back-end.[7] TS identified using pyGSM were re-optimized in Jaguar to ensure consistency. To reduce computational costs, these calculations were conducted using the range-separated hybrid generalized gradient approximation (GGA) density functional ωB97X-D,[8] def2-SVPD basis set,[9,10] and Conductor-like Screening Model (COSMO)[11,12] implementation of the po-

larizable continuum model (PCM)[13] with water as the solvent. In Jaguar, all basis functions representing f and higher orbitals were removed to further reduce cost, making the basis more precisely def2-SVPD(-f). All TS were confirmed to have one imaginary frequency and to connect to the expected endpoints. The electronic energies of all TS and reaction endpoints (reactants and products) were corrected with single-point energy evaluations in Jaguar using range-separated hybrid meta-GGA functional ωB97M-V with the def2-TZVPD basis set in COSMO. Note that ωB97X-D and ωB97M-V density functionals perform excellently on benchmarks of reaction energies and energy barriers.[14]

In general, reaction free energies ΔG and energy barriers $\Delta G^{\ddagger}$ are reported using the calculated Gibbs free energies of the optimized reaction entrance and exit complexes (as opposed to the isolated reactants and products at infinite separation). Some exceptions are made, for instance in the case where optimization of an endpoint fails due to multiple fragments flying away towards infinite separation. In all reported reaction mechanisms, species not prefixed by "M" - for example, $LiPF_2O_2 + PF_5$ in Figure 4 of the main text - indicate that an infinite separation approximation was used.

In the energy diagrams shown in the main text, there are several reactions where species are removed. For example, in Figure 1 of the main text, HF is removed in the reaction $M_2 \longrightarrow M_3$, and in Figure 2 of the main text, LiF is removed in the reactions $M_8 \longrightarrow M_9$ and $M_{12} \longrightarrow M_{13}$. In all such cases, we assume that the removal of those dissociated species from the reacting complex is isergonic ($\Delta G = 0.0$ eV), and we do not show the complex without the removed species in the energy diagrams. However, as we note above (see Data Availability), we always performed optimizations on the associated reaction endpoints with and without the removed species (HF, LiF, and/or CO_2) as part of our process to verify TS.

For correlation plots between reaction energy and partial charge, partial charges were obtained using the Natural Bonding Orbital (NBO)[15] program version 7.0.[16] For the species considered in the main text (Li_2CO_3, $LiHCO_3$, and H_2CO_3), single-point energy evaluations were performed on structures from the Lithium-Ion Battery Electrolyte (LIBE) dataset[17]

using the ωB97X-V range-separated hybrid GGA functional,[18] def2-TZVPPD basis set,[10] and SMD implicit solvent model[19] (with EC/EMC as the solvent).[17] Unless otherwise noted, only the partial charges of the most negatively charged oxygen atoms are reported.

Rate coefficients reported in the main text are calculated using the Eyring equation:

$$k = \frac{k_B T}{h} exp(\frac{-\Delta G^{\ddagger}}{k_B T}) \tag{1}$$

where k_B is the Boltzmann constant, h is the Planck constant, $\Delta G^{\ddagger}$ is the reaction energy barrier, and T is the absolute temperature.

Reactions with bulk lithium carbonate

The calculations performed in this study use an implicit solvent environment. Therefore, the mechanisms that we describe for the reaction of $LiPF_6$ and its decomposition products with Li_2CO_3 most directly describe reactions in solution. However, Li_2CO_3 is highly insoluble in carbonate electrolytes,[20] so we should expect that $LiPF_6$ is more likely to interact with solid Li_2CO_3 than Li_2CO_3 in solution. We therefore consider if $LiPF_6$ can react with solid Li_2CO_3.

Experimentally, is has been found that solid, insoluble Li_2CO_3 can chemically react with $LiPF_6$ at moderate temperatures.[21,22] Without further study, we cannot say for certain that solution-phase and solid-phase Li_2CO_3 react via the same mechanism. However, we believe that, regardless of possible mechanistic differences, the addition of PF_5 and POF_3 to solid Li_2CO_3 should be favorable.

The SEI is typically amorphous or comprised of nanocrystalline domains,[23] so we expect that there will be no shortage of reactive ${CO_3}^{2-}$ in the Li_2CO_3 regions at domain/grain boundaries and defects. To further support our hypothesis, we examined the atomic partial charges of oxygens in Li_2CO_3 clusters simulating amorphous and nanocrystalline regions.

We obtained the crystal structure of monoclinic Li_2CO_3 from the Materials Project (mp-

3054).[24] Using this crystal structure, we constructed structures composed of 2, 4, 10, and 16 Li_2CO_3. These structures are meant to simulate nanoscale crystalline domains. To approximate an amorphous Li_2CO_3 environment, we generated a random box containing four Li_2CO_3 units via PACKMOL.[25] We then obtained the partial charges for the nanocrystalline and amorphous structures via NBO analysis at the ωB97X-V/def2-TZVPPD/SMD level of theory, as described above. The results are listed in Table S1.

Table S1: **Average oxygen atomic partial charge $q_{O,avg}$ for clusters of Li_2CO_3.**

# Li_2CO_3	$q_{O,avg}$
1	-0.94
2	-0.97
4	-0.95
4 (random)	-0.94
10	-0.96
16	-0.95

The average oxygen partial charge in isolated Li_2CO_3 is -0.94. For the amorphous structure (indicated as "random"), the average oxygen partial charge is also -0.94, while for the nanocrystalline samples the average ranged from -0.95 to -0.97. In effect, it appears that the charge distribution within CO_3^{2-} units does not change as the cluster size increases. Since our analysis suggests that PF_5 and POF_3 prefer adding to highly anionic oxygens, this indicates that bulk amorphous or nanocrystalline Li_2CO_3 should be effectively just as reactive as isolated Li_2CO_3. As we note in the main text, reactions occurring within the SEI will depend on the porosity of the interphase and the transport of PF_6^-.

On the selectivity of phosphorus fluoride reactivity

As we discussed in the main text, POF_3 reacts selectively, preferring to add to Li_2CO_3 rather than $LiHCO_3$ or H_2CO_3. We attribute this to the anionic character and the basicity of the reacting oxygens. This trend not only holds for POF_3, but also for PF_5, as we show in Figure S1.

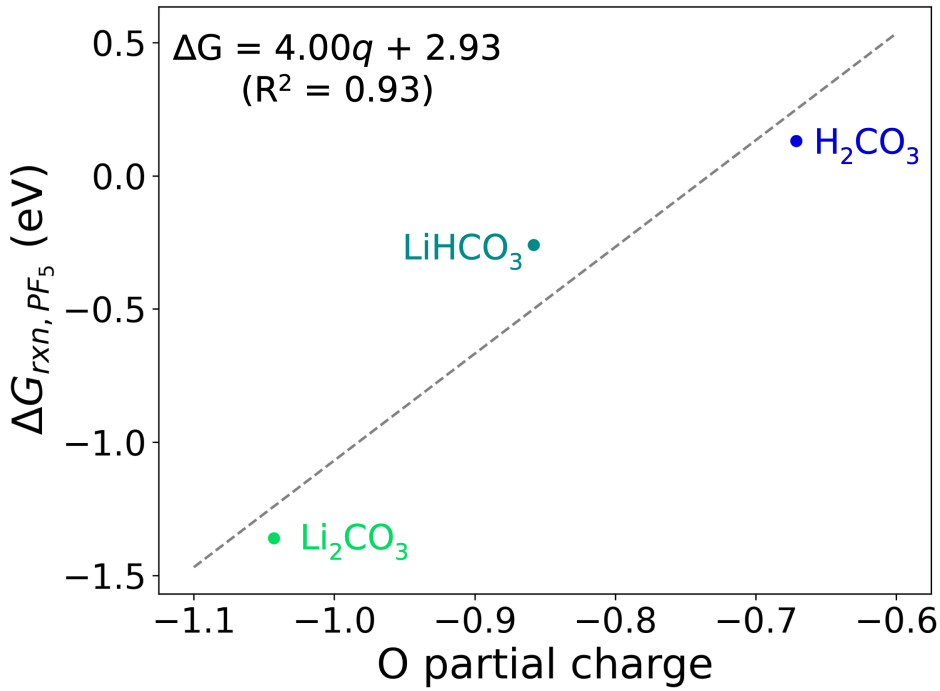

Figure S1: Reaction free energies in the reaction $\mathrm{RR'CO_3 + PF_5 \longrightarrow ROCOR'OPF_5}$, where R, R′ = H, Li as a function of the partial charge of the reacting oxygen(s) in the inorganic carbonate species. A linear fit, $\Delta G = 4.00q + 2.93$ ($R^2 = 0.93$), where q = the most negative oxygen partial charge, is provided.

The observed selectivity of neutral phosphorus fluoride reactivity appears to be at least somewhat general, raising a question: is this selectivity species-specific, or can species such as PF_5 and POF_3 react with any oxyanion with sufficiently charged oxygens?

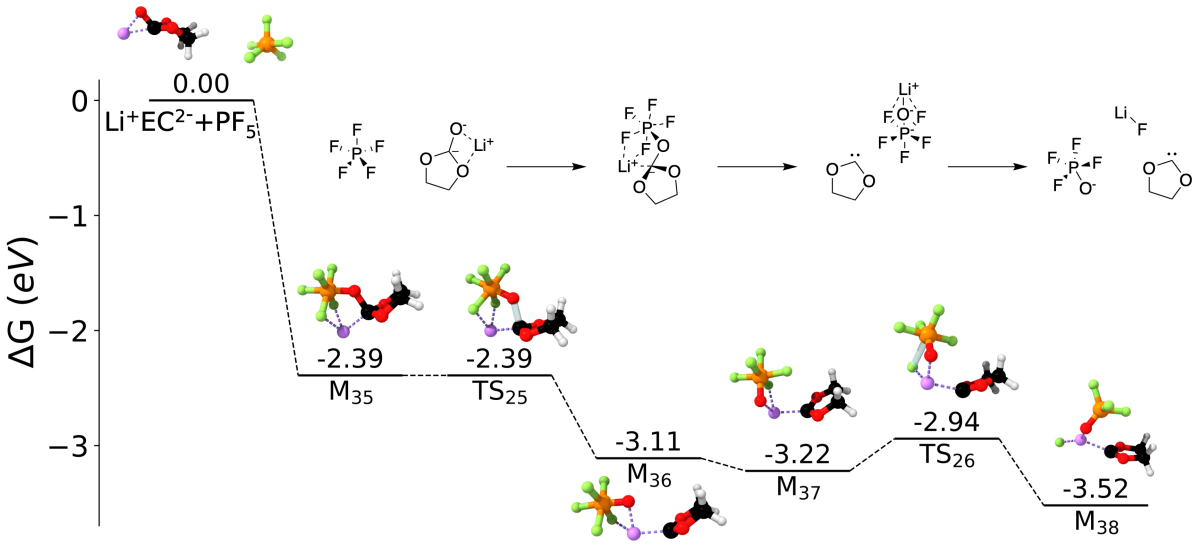

Figure S2: Reaction mechanism between PF_5 and Li^+EC^{2-}. Following a highly exergonic ($\Delta G = -2.39$ eV) and barrierless addition step, $LiPF_5O^-$ is eliminated to form the 1,3-dioxolylidene carbene in another essentially barrierless reaction ($\Delta G^\ddagger < 0.01$ eV). Finally, $LiPF_5O$ can eliminate LiF to form $POF_4{}^-$; upon coordination with Li^+, this could form POF_3 and an additional LiF as shown in Figure 2 of the main text.

While we have not exhaustively explored the reactivity of PF_5, POF_3, or related species, Figure S2 provides evidence that oxyanions other than $CO_3{}^{2-}$ can react favorably with PF_5. Specifically, we predict that PF_5 can react with Li^+EC following two-electron reduction (Li^+EC^{2-}). The reacting oxygen in Li^+EC^{2-} has a similar partial charge to the reacting oxygen in Li_2CO_3 as calculated using NBO (-1.04). The addition reaction - $PF_5 + Li^+EC^{2-} \longrightarrow M_{34}$ - is barrierless and even more exergonic than the reaction between PF_5 and Li_2CO_3 ($\Delta G = -2.39$ eV, compared with $\Delta G = -1.36$ eV for the reaction with Li_2CO_3). Following addition, $LiPF_5O^-$ is eliminated ($\Delta G^\ddagger < 0.01$ eV, $\Delta G = -0.72$ eV), yielding a carbene (1,3-dioxolylidene, also known as dioxolylidene). $LiPF_5O^-$ can then eliminate LiF, forming first $POF_4{}^-$ and then, via a pathway like that shown in Figure 2 of the main text, POF_3 (not shown in Figure S2).

We note that this is not by any means a far-fetched example. In regimes with rapid electron transfer (during early SEI formation close to the electrode, or under extremely low applied potentials), the two-electron reduction reaction to form ($Li^{+}EC^{2-}$) is favorable and could even dominate over other reduction pathways.[26,27] We have even previously predicted dioxolylidene to form as an intermediate during SEI formation,[28] though we suspect that it should not be stable and should eventually decompose.

References

(1) Spotte-Smith, E. W. C.; Petrocelli, T. B.; Petal, H. D.; Blau, S. M.; Persson, K. A. Data for "Elementary Decomposition Mechanisms of Lithium Hexafluorophosphate in Battery Electrolytes and Interphases". 2022; DOI:10.6084/m9.figshare.21583581.v1.

(2) Ong, S. P.; Richards, W. D.; Jain, A.; Hautier, G.; Kocher, M.; Cholia, S.; Gunter, D.; Chevrier, V. L.; Persson, K. A.; Ceder, G. Python Materials Genomics (pymatgen): A robust, open-source python library for materials analysis. *Computational Materials Science* **2013**, *68*, 314–319.

(3) Jacobson, L. D.; Bochevarov, A. D.; Watson, M. A.; Hughes, T. F.; Rinaldo, D.; Ehrlich, S.; Steinbrecher, T. B.; Vaitheeswaran, S.; Philipp, D. M.; Halls, M. D.; Friesner, R. A. Automated Transition State Search and Its Application to Diverse Types of Organic Reactions. *J. Chem. Theory Comput.* **2017**, *13*, 5780–5797.

(4) Bochevarov, A. D.; Harder, E.; Hughes, T. F.; Greenwood, J. R.; Braden, D. A.; Philipp, D. M.; Rinaldo, D.; Halls, M. D.; Zhang, J.; Friesner, R. A. Jaguar: A high-performance quantum chemistry software program with strengths in life and materials sciences. *International Journal of Quantum Chemistry* **2013**, *113*, 2110–2142.

(5) Zimmerman, P. M. Single-ended transition state finding with the growing string method. *Journal of Computational Chemistry* **2015**, *36*, 601–611.

(6) Aldaz, C. Development of Reaction Discovery Tools in Photochemistry and Condensed Phases. Thesis, 2020.

(7) Epifanovsky, E. et al. Software for the frontiers of quantum chemistry: An overview of developments in the Q-Chem 5 package. *J. Chem. Phys.* **2021**, *155*, 084801.

(8) Chai, J.-D.; Head-Gordon, M. Long-range corrected hybrid density functionals with damped atom–atom dispersion corrections. *Physical Chemistry Chemical Physics* **2008**, *10*, 6615–6620.

(9) Weigend, F.; Ahlrichs, R. Balanced basis sets of split valence, triple zeta valence and quadruple zeta valence quality for H to Rn: Design and assessment of accuracy. *Physical Chemistry Chemical Physics* **2005**, *7*, 3297–3305.

(10) Rappoport, D.; Furche, F. Property-optimized Gaussian basis sets for molecular response calculations. *J. Chem. Phys.* **2010**, *133*, 134105.

(11) Klamt, A.; Schüürmann, G. COSMO: a new approach to dielectric screening in solvents with explicit expressions for the screening energy and its gradient. *Journal of the Chemical Society, Perkin Transactions 2* **1993**, *0*, 799–805.

(12) Klamt, A. The COSMO and COSMO-RS solvation models. *WIREs Computational Molecular Science* **2011**, *1*, 699–709.

(13) Mennucci, B. Polarizable continuum model. *WIREs Computational Molecular Science* **2012**, *2*, 386–404.

(14) Mardirossian, N.; Head-Gordon, M. Thirty years of density functional theory in computational chemistry: an overview and extensive assessment of 200 density functionals. *Molecular Physics* **2017**, *115*, 2315–2372.

(15) Glendening, E. D.; Landis, C. R.; Weinhold, F. Natural bond orbital methods. *WIREs Computational Molecular Science* **2012**, *2*, 1–42.

(16) Glendening, E. D.; Landis, C. R.; Weinhold, F. NBO 7.0: New vistas in localized and delocalized chemical bonding theory. *Journal of Computational Chemistry* **2019**, *40*, 2234–2241.

(17) Spotte-Smith, E. W. C.; Blau, S. M.; Xie, X.; Patel, H. D.; Wen, M.; Wood, B.; Dwaraknath, S.; Persson, K. A. Quantum chemical calculations of lithium-ion battery electrolyte and interphase species. *Sci Data* **2021**, *8*, 203, Number: 1 Publisher: Nature Publishing Group.

(18) Mardirossian, N.; Head-Gordon, M. B97X-V: A 10-parameter, range-separated hybrid, generalized gradient approximation density functional with nonlocal correlation, designed by a survival-of-the-fittest strategy. *Phys. Chem. Chem. Phys.* **2014**, *16*, 9904–9924.

(19) Marenich, A. V.; Cramer, C. J.; Truhlar, D. G. Universal Solvation Model Based on Solute Electron Density and on a Continuum Model of the Solvent Defined by the Bulk Dielectric Constant and Atomic Surface Tensions. *J. Phys. Chem. B* **2009**, *113*, 6378–6396.

(20) Tasaki, K.; Goldberg, A.; Lian, J.-J.; Walker, M.; Timmons, A.; Harris, S. J. Solubility of lithium salts formed on the lithium-ion battery negative electrode surface in organic solvents. *Journal of The Electrochemical Society* **2009**, *156*, A1019.

(21) Bi, Y.; Wang, T.; Liu, M.; Du, R.; Yang, W.; Liu, Z.; Peng, Z.; Liu, Y.; Wang, D.; Sun, X. Stability of Li2CO3 in cathode of lithium ion battery and its influence on electrochemical performance. *RSC Adv.* **2016**, *6*, 19233–19237.

(22) Parimalam, B. S.; MacIntosh, A. D.; Kadam, R.; Lucht, B. L. Decomposition Reactions of Anode Solid Electrolyte Interphase (SEI) Components with LiPF6. *J. Phys. Chem. C* **2017**, *121*, 22733–22738.

(23) Bhattacharya, S.; Alpas, A. T. Micromechanisms of solid electrolyte interphase formation on electrochemically cycled graphite electrodes in lithium-ion cells. *Carbon* **2012**, *50*, 5359–5371.

(24) Jain, A.; Ong, S. P.; Hautier, G.; Chen, W.; Richards, W. D.; Dacek, S.; Cholia, S.; Gunter, D.; Skinner, D.; Ceder, G., et al. Commentary: The Materials Project: A materials genome approach to accelerating materials innovation. *APL materials* **2013**, *1*, 011002.

(25) Martínez, L.; Andrade, R.; Birgin, E. G.; Martínez, J. M. PACKMOL: A package for building initial configurations for molecular dynamics simulations. *Journal of computational chemistry* **2009**, *30*, 2157–2164.

(26) Leung, K. Two-electron reduction of ethylene carbonate: A quantum chemistry re-examination of mechanisms. *Chemical Physics Letters* **2013**, *568-569*, 1–8.

(27) Spotte-Smith, E. W. C.; Kam, R. L.; Barter, D.; Xie, X.; Hou, T.; Dwaraknath, S.; Blau, S. M.; Persson, K. A. Toward a Mechanistic Model of Solid–Electrolyte Interphase Formation and Evolution in Lithium-Ion Batteries. *ACS Energy Lett.* **2022**, *7*, 1446–1453.

(28) Barter, D.; Spotte-Smith, E. W. C.; Redkar, N. S.; Khanwale, A.; Dwaraknath, S.; Persson, K. A.; Blau, S. M. Predictive stochastic analysis of massive filter-based electrochemical reaction networks. *ChemRxiv* **2022**, DOI: 10.26434/chemrxiv-2021-c2gp3-v3.